Inorganic Chemistry Communications 183 (2026) 115873

Contents lists available at ScienceDirect

Inorganic Chemistry Communications

journal homepage: www.elsevier.com/locate/inoche

Research Article

Synthesis, spectroscopic and single-crystal analysis, and DFT studies of N_2O_2 diamine coordination complexes: solvent-driven geometry switching and NLO properties

Jasim M.S. Alshawi [a], Baidaa K. Al-Rubaye [b], Hanadi M. Jarallah [a], Sadiq M.-H. Ismael [a], Mohamad J. Al-Jeboori [b,*], Inigo J. Vitorica-Yrezabal [c], Richard E.P. Winpenny [c,*]

[a] Department of Chemistry, College of Education for Pure Science, University of Basrah, Iraq
[b] Department of Chemistry, College of Education for Pure Science (Ibn Al-Haitham), University of Baghdad, Baghdad, Iraq
[c] Department of Chemistry, School of Natural Sciences, University of Manchester, Oxford Road, Manchester M13 9PL, United Kingdom

ARTICLE INFO

Keywords:
Tetradentate N_2O_2 ligand
Diamine-based complexes
X-ray crystallography
Solvent-driven geometry transformation
DFT studies
Nonlinear optical properties

ABSTRACT

The design of coordination compounds with solvent-responsive optical properties remains a central challenge in molecular photonics. Here, we describe the synthesis and full characterisation of a symmetrical tetradentate diamine ligand, 3,3′-((1,2-phenylenebis(azanediyl))- bis(methanylylidene))bis(pentane-2,4-dione) (H_2L), and its neutral square-planar complexes [M(L)] (M(II) = Co, Ni, Cu). The Cu(II) complex crystallised as [Cu(L)]·0.5 (pyrazine), adopting a nearly square-planar geometry ($\tau_4 = 0.06$) in the solid state, as confirmed by single-crystal X-ray diffraction. In DMSO solution, UV–Vis spectra revealed reversible axial coordination of two solvent molecules, driving a transformation to a distorted octahedral geometry. Structural assignments were supported by FT-IR, UV–Vis, NMR, ESI-MS, conductivity, and magnetic susceptibility measurements. Density functional theory (DFT) calculations (B3LYP/6-311 + G(d,p) for H_2L; LANL2DZ for the complexes) reproduced the experimental geometries, mapped frontier orbital distributions, and yielded global reactivity descriptors. Among the complexes, [Cu(L)] displayed the narrowest HOMO–LUMO gap ($\Delta E = 3.911$ eV), the highest polarisability ($\alpha = 305.3$ a.u.), and an exceptionally large second-order hyperpolarisability ($\beta = 2.20 \times 10^4$ a.u.), surpassing benchmark compounds such as urea, *p*-nitroaniline (pNA), and 2-methyl-4-nitroaniline (MNA) by more than 50 %. These results highlight diamine-derived N_2O_2 frameworks as promising candidates for solvent-responsive nonlinear optical (NLO) materials, combining hydrolytic stability with geometry switching and enhanced second-order optical performance. Importantly, X-ray data reveal that coordination to Cu(II) induces electron redistribution, imparting imine-like character to the nitrogen donors despite the diamine nature of the free ligand. This interplay highlights both the novelty and the performance advantage of the present system within the second-order NLO domain of Cu(II) complexes.

1. Introduction

Coordination chemistry has grown steadily in recent decades, reflecting the sustained importance of metal-based compounds in science, technologies, and industry. This growth has closely followed progress in synthetic organic chemistry, which continues to inspire new and more efficient methods of synthesis [1–3]. Much of this work is directed toward designing and improving pathways for small organic molecules containing donor atoms that act as coordination centres [4–7]. The synthesis of polydentate ligands and their coordination complexes, whether containing homo- or hetero-donor atoms, continues to occupy a central position in coordination chemistry [8–11]. Multidentate ligands, particularly those with N_2O_2 frameworks, form highly stable metal complexes owing to the chelation effect [12]. Such structures are thermodynamically robust and are used in electronic, photonic, and nonlinear optical (NLO) applications [13,14]. Complexes of this type have also found broad use in catalysis, analytical and biomedical chemistry, photophysical and electrochemical studies, and environmental remediation [15–19]. Both symmetric and asymmetric N_2O_2 frameworks derived from Schiff bases or amine-type ligands have

* Corresponding authors.
E-mail addresses: mohamad.al-jeboori@ihcoedu.uobaghdad.edu.iq (M.J. Al-Jeboori), richard.winpenny@manchester.ac.uk (R.E.P. Winpenny).

https://doi.org/10.1016/j.inoche.2025.115873
Received 28 September 2025; Received in revised form 5 November 2025; Accepted 19 November 2025
Available online 20 November 2025

also been widely reported [11,20–23]. Foundational investigations of *cis*-[N_2O_2] metal chelate systems have provided key insights into their coordination behaviour, solid-state and spectroscopic characteristics [22,24].

Within this class, both symmetric and asymmetric multidentate ligands with hetero-donor atoms such as N_2S_2, N_2O_2, and N_2O_4, including Schiff bases, have been widely explored as chelation agents [6,9,12,25,26]. Schiff base complexes with an N_2O_2 donor set are particularly well known for their NLO properties, which arise mainly from their square-planar geometry. The rigid planar framework favours charge delocalisation and, in turn, enhances NLO responses [27]. X-ray single-crystal structures of nickel(II) and copper(II) Schiff base complexes support this behaviour, showing square-planar coordination that is consistent with enhanced NLO activity. Moreover, square-planar *trans*-[MN_2O_2] complexes exhibit third-order polarisability (γ) values that are substantially higher than those of standard NLO reference materials [28].

Despite these advances, the broader application of Schiff base complexes is limited by hydrolytic instability and restricted structural flexibility. The susceptibility of the imine (–C=N–) bond to hydrolysis, particularly in polar or aqueous environments, and the absence of reversible coordination, both hinder their use in dynamic optical materials [29]. In contrast, diamine-derived N_2O_2 frameworks provide greater hydrolytic stability and reversible coordination behaviour. Although distinct from classical Schiff bases, coordination to Cu(II) can induce partial imine-like donor character in the nitrogen donors, enhancing their similarity to N_2O_2 systems with established NLO activity. While the free ligand behaves as a diamine in nature, as confirmed by NMR and FT-IR spectra, coordination to Cu(II) promotes deprotonation and electron redistribution so that the nitrogen donors acquire imine-like properties, consistent with the observed contraction of the C—N bond in the X-ray structure. Despite these favourable features, the potential of diamine-derived N_2O_2 scaffolds for NLO applications remains largely unexplored. This gap in the literature provides motivation for the present study.

To fill this gap, we have synthesised and characterised a symmetrical diamine-based tetradentate ligand bearing an N_2O_2 core, along with its Co(II), Ni(II), and Cu(II) complexes. In solution, these complexes undergo a reversible transformation in geometry, from square-planar in the solid state to octahedral upon DMSO coordination, as a result of weak axial solvent binding (see Results for structural data). We combined experimental characterisation with density functional theory (DFT) simulations to investigate this solvent-driven switching and quantify the second-order NLO response. The results confirm the structural transformation and reveal a strong second-order NLO response that exceeds benchmark chromophores such as urea, *p*-nitroaniline, and 2-methyl-4-nitroaniline (see Results and Methods).

In summary, our experimental and theoretical results show that diamine-derived N_2O_2 scaffolds can overcome the hydrolytic and structural limitations of classical imine-derived systems and provide a robust and tunable platform for solvent-switchable NLO materials.

2. Experimental

2.1. Materials and solvent treatment

All solid chemicals and solvents were obtained from Merck or Sigma-Aldrich and used without further purification. Solvents were of analytical grade and used as supplied: absolute ethanol (Merck, ≥ 99.8 %), methanol (Merck, ≥ 99.9 %), dichloromethane (Merck, ≥ 99.8 %), and diethyl ether (Merck, ≥ 99.5 %).

Reagents and their suppliers were as follows: 3-(ethoxymethylene) pentane-2,4-dione (Sigma-Aldrich, ≥ 95 %), *o*-phenylenediamine (Sigma-Aldrich, ≥ 98 %), copper(II) chloride dihydrate (Sigma-Aldrich, ≥ 99.0 %), cobalt(II) chloride hexahydrate (Merck), nickel(II) chloride hexahydrate (Merck, ≥ 98 %), glacial acetic acid (Merck, ≥ 99.7 %), *N*, *N*-dimethylformamide (Merck, ≥ 99.8 %), and potassium bromide for FT-IR pellets (Sigma-Aldrich, ≥ 99 %).

2.2. Instrumentation and measurements

Elemental analyses (C, H, N) were performed on a EuroEA 3000 elemental analyser (EuroVector), and metal contents were determined by atomic absorption spectroscopy (AAS) on a Shimadzu atomic absorption spectrometer. Chloride percentages were measured by potentiometric titration using a Metrohm 686 Titroprocessor equipped with a 665 Dosimat burette. Melting points (uncorrected) were recorded on a Thermo Scientific melting point apparatus. FT-IR spectra (KBr pellet) were collected on a Shimadzu FTIR-8400S over 4000–400 cm^{-1}. ^1H and ^{13}C NMR spectra were acquired on a Bruker Avance 400 MHz spectrometer in DMSO-d_6, referenced to residual DMSO (^1H 2.50 ppm, ^{13}C 39.52 ppm). UV–Vis spectra were measured in DMSO on a U·V-win5 spectrophotometer using 10 mm quartz cuvettes (200–800 nm). ESI-MS (positive mode) was recorded on a Waters ACQUITY UPLC SQ detector with sample infusion at 10 μL min^{-1}. Molar conductivities (Λm) were measured for 10^{-3} M solutions in DMSO at 25 °C using a WTW conduct meter, and magnetic susceptibilities of the solid complexes were determined at 298 K using a Sherwood Scientific magnetic susceptibility balance calibrated with Hg[Co(SCN)$_4$].

2.3. Synthesis

2.3.1. Synthesis of the ligand (H_2L)

A conventional method reported in [30] was implemented with modifications to prepare the ligand as follows:

To a mixture of 3-(ethoxymethylene)pentane-2,4-dione (3.124 g, 20 mmol) in ethanol (20 mL) containing three drops of glacial acetic acid, a solution of *o*-phenylenediamine (0.500 g, 5 mmol) in ethanol (20 mL) was added dropwise with stirring over 20 min. The reaction mixture was refluxed for 3 h and then cooled to room temperature. A pale yellow precipitate was collected by filtration and recrystallised from ethanol, yielding 1.18 g (65 %), m.p. 175–177 °C. FT-IR (ν, cm^{-1}): 3377 ν(N—H), 1707, 1688 ν(C=O), 1618 ν(C=C, aromatic), 1300 ν(C—N). ^1H NMR (DMSO-d_6, 400 MHz, δ ppm): 10.11 (2H, s, N—H), 8.52 (2H, s, C4,4′–H–N), 7.65–7.63 (2H, d, C2,2′–H, J = 8.3 Hz), 7.46–7.40 (2H, m, C3,3′–H), 2.14 (12H, s, 4CH_3), ~2.50 (DMSO solvent), ~3.41 (trace water). ^{13}C NMR (DMSO-d_6, 100.63 MHz, δ ppm): 196.59 (C=O), 160.30 (C4,4′), 129.33 (C1,1′), 121.69 (C3,3′), 112.97 (C2,2′), 108.45 (C5,5′), 30.66 (methyl groups). ESMS(+): m/z: 329.2 $[M]^+$, 200, 128, 102. UV–Vis (DMSO, nm): 305 ($\pi \rightarrow \pi^*$).

2.3.2. Synthesis of metal complexes

A solution of $CuCl_2{\cdot}2H_2O$ (0.1705 g, 1 mmol) was added dropwise with stirring to a solution of H_2L (0.329 g, 1 mmol) in a methanol/ethanol/DMF mixture (16 mL, 3:3:2, *v*/v). The reaction mixture was stirred for 10 min and refluxed for 30 min. The hot solution was filtered and allowed to evaporate slowly at room temperature. A red-brown powder of the Cu(II) complex was obtained. The solid was washed sequentially with cold water (5 mL), cold methanol (3 mL), and diethyl ether (5 mL), then dried under vacuum, affording 0.254 g (63 %). Red crystals suitable for single-crystal X-ray analysis were grown by slow diffusion of diethyl ether into a dichloromethane solution of the complex.

An analogous method was used to synthesise the Co(II) and Ni(II) complexes. Their physical data and yields are listed in Table 1.

2.4. X-ray single-crystal diffraction

The single-crystal X-ray diffraction data for the copper(II) coordination complex [Cu(L)] were collected on a SuperNova diffractometer equipped with Mo Kα radiation (λ = 0.71073 Å) at 150 K under a nitrogen stream supplied by an Oxford Cryosystems 700 Series

Table 1
Elemental microanalyses and other analytical data of H_2L and its coordination compounds.

Compound	m.p. (°C)	Colour	Yield (%)	M.wt	Found (calc.) %			
					C	H	N	M
H_2L	175–177	Yellow powder	65	328.00	65.77 (65.84)	6.26 (6.14)	8.48 (8.53)	–
[Co(L)]	>300*	Dark green	59	386.10	56.11 (55.97)	4.96 (5.21)	7.19 (7.25)	15.31 (15.26)
[Ni(L)]	>300*	Bright yellow	58	385.1	55.93 (56.00)	4.88 (4.96)	7.23 (7.26)	15.17 (15.20)
[Cu(L)]·0.5(pyrazine)	>300*	Red-brown	63	429.94	55.82 (55.87)	4.90 (4.88)	9.73 (9.76)	14.77 (14.72)

*Decomposed.

Cryostream. A suitable crystal was mounted on a glass fibre. Data reduction and unit cell refinement were carried out using CrystalClear SM-Expert (Rigaku, The Woodlands, TX, USA). An empirical absorption correction was applied using SADABS (Bruker). The structure was solved by direct methods using SHELXS and refined by full-matrix least-squares on F^2 using SHELXL [31], both accessed through the OLEX2 interface [32]. All non-hydrogen atoms were refined anisotropically. Molecular graphics and structural analysis were performed using OLEX2 [32].

2.5. Theoretical approach

Density Functional Theory (DFT) calculations were carried out to complement the structural data obtained from X-ray crystallography. All computations were performed using Gaussian 16, revision A.03 [33]. Geometry optimisation of the ligand and its metal complexes was conducted using the B3LYP functional, with 6–311 + G(d,p) applied for the ligand and LANL2DZ for the coordination compounds [4,5,34]. The simulations provided insight into the electronic structure by evaluating the frontier molecular orbitals, namely the highest occupied (HOMO) and lowest unoccupied (LUMO) orbitals, and calculating the HOMO-LUMO gap (ΔE). Additional descriptors, such as global softness (S, eV^{-1}) and hardness (η, eV), were also determined [35a]. These parameters are widely used to characterise chemical reactivity and stability. Molecular electrostatic potential (MEP) maps were generated from electron density distributions to highlight regions of electron excess and deficiency. The resulting surface plots helped identify possible electrophilic and nucleophilic sites by indicating areas of negative (red) and positive (blue) potential [35b].

3. Results and discussion

3.1. Synthesis

The ligand H_2L was obtained by reacting 3-(ethoxymethylene) pentane-2,4-dione with *o*-phenylenediamine in ethanol, using a few drops of glacial acetic acid as a catalyst (Scheme 1). The product was isolated as a pale yellow solid, readily soluble in DMSO and DMF but only sparingly soluble in other common organic solvents. Its structure contains two labile protons, which, upon deprotonation, allow the ligand to function as a dibasic tetradentate chelating agent with an N_2O_2 donor set.

The ligand was subsequently reacted with the chloride salts of Co(II), Ni(II), and Cu(II) in a mixed solvent system of methanol, ethanol, and DMF (3:3:2 *v*/v), which proved essential for complete reaction (Scheme 2). Elemental microanalysis (CHN) and metal content values were in good agreement with the calculated values (Table 1), confirming the stoichiometry and purity of the compounds.

FTIR spectra (Table 2) showed a downshift of one ν(C=O) band relative to the free ligand. This observation is consistent with coordination through the oxygen donor atoms. The UV–Vis spectra (Table 3) contained absorption bands characteristic of d-d transitions together with metal-to-ligand charge-transfer features, reflecting changes in coordination geometry in solution. Potentiometric titration of the complexes and their filtrates gave no evidence of chloride ions, confirming that chloride was completely displaced during complexation. Molar conductance values of 10.1, 7.6, and 9.5 S cm^2 mol^{-1} for the Co(II), Ni(II), and Cu(II) complexes, respectively, confirmed their non-electrolytic nature. Together, these findings indicate the formation of neutral, four-coordinate species with square-planar geometry around the metal centres. The geometry was further established by single-crystal X-ray diffraction of the [Cu(L)] complex.

3.2. FT-IR data

The FT-IR spectrum of the free ligand (H_2L) is shown in **Fig. S1** and summarised in Table 2. A broad band at 3377 cm^{-1} was assigned to the N—H stretching vibration of the secondary amine, indicating that the ligand is a diamine rather than a Schiff base. Two strong carbonyl bands were observed at 1707 and 1688 cm^{-1}, suggesting that the two carbonyl groups occupy slightly different environments [9,30].

In the FT-IR spectra of the coordination compounds, the N—H peak was absent (**Figs. S2–S4**). This finding is consistent with deprotonation and subsequent coordination through the nitrogen atoms. In the carbonyl region, the complexes exhibited two bands: one remaining near 1707 cm^{-1} (unbound C=O) and the other shifting to around 1670 cm^{-1}, attributed to a coordinated carbonyl oxygen to the metal centre. This downshift of 16–27 cm^{-1} suggests partial π-back bonding and a reduction of the C=O bond [25,26]. This interpretation is supported by

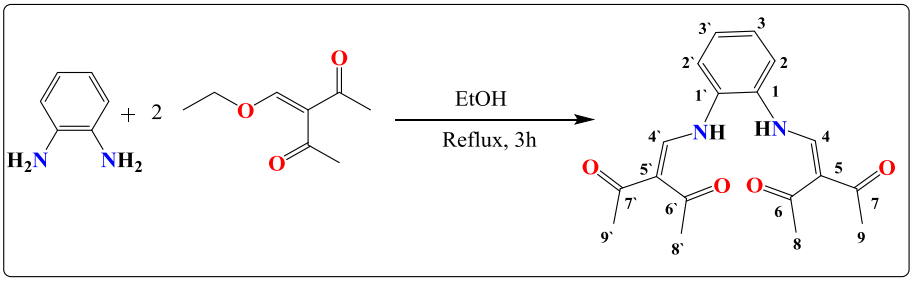

Scheme 1. Synthesis pathway of the ligand (H_2L).

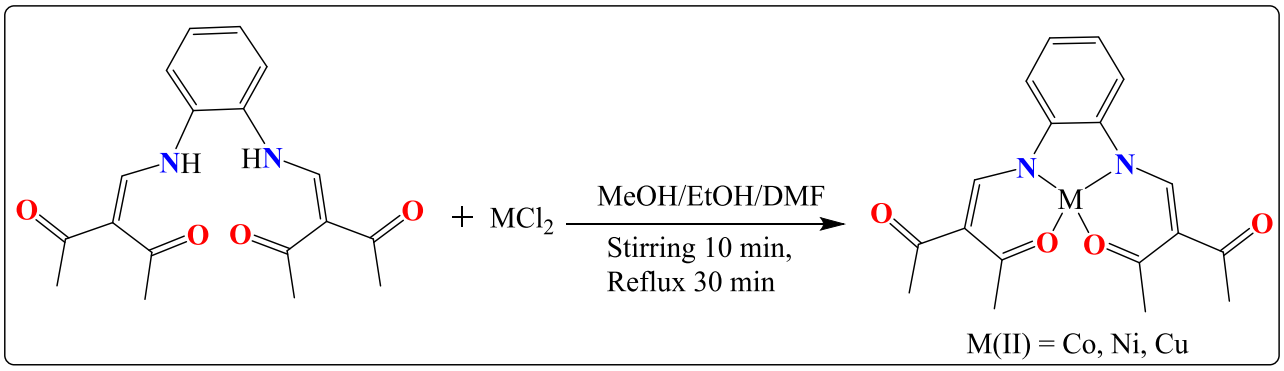

Scheme 2. Synthesis pathway for the coordination complexes.

Table 2
FTIR values (cm^{-1}) of H_2L and coordination complexes.

Vibration mode	H_2L	[Co(L)]	[Ni(L)]	[Cu(L)]
ν(C=O) (coordinated)	–	1668	1661	1672
ν(C=O) (uncoordinated)	1707, 1688	1708	1705	1707
ν(C=C)	1618	1631	1630, 1621	1631, 1622
ν(C—C)	1539	1442	1450	1442
ν(C—N)	1300	1257	1262	1257
ν(M-O)	–	602	587	518
ν(M-N)	–	508	496	482

Table 3
Electronic spectral data for H_2L and coordination complexes.

Compound	Magnetic moment (BM)	Band position (nm)	λ (cm^{-1})	Molar absorptivity ε_{max} ($dm^3mol^{-1}cm^{-1}$)	Suggested transition
H_2L	–	305	32,786	1300	π → π*, n → π* (ligand field)
[Co(L)]	1.75	275 361 669	36,363 27,698 14,949	1030 44 150	Ligand field ligand-to-metal charge transfer (LMCT). $^2E \rightarrow {}^2T_2g$
[Ni(L)]	0.4	300 508	33,333 19,685	1160 21	Ligand field $^3A_2g \rightarrow {}^3T_1g^{(P)}$
[Cu(L)]	1.84	290 620	34,483 16,129	1261.9 54	Ligand field $^2B_1g \rightarrow {}^2E_g$ or $^2B_1g \rightarrow {}^2B_2g$

molecular orbital analysis. DFT calculations showed the HOMO of the Cu(II) complex spread over the aromatic system and extending into the coordinated carbonyls, consistent with strong delocalisation and d–π to p–π* overlap. X-ray crystallography (Table 5) provided further evidence: the C═O bond lengths for coordinated sites (C11–O12 = 1.273(3) Å; C22–O23 = 1.279(3) Å) were longer than those of the unbound groups (C13–O14 = 1.224(3) Å; C20–O21 = 1.208(4) Å), supporting electron donation from the metal into the ligand's p-π* orbitals. New bands between 602 and 587 cm^{-1} and 518–482 cm^{-1} were observed in the complexes and were assigned to M–O and M–N stretching vibrations, respectively [6,7–9,36], providing further confirmation of coordination through both oxygen and nitrogen. The relatively higher frequency of the M–O bands is consistent with the larger dipole moment change associated with M–O bond stretching [36].

3.3. NMR and mass spectroscopy data

The ^1H and ^{13}C NMR spectra of H_2L were recorded in DMSO-d_6 and assigned according to Scheme 1. All expected signals were present with correct integrations, and no additional peaks were detected, indicating the presence of a single isomer in solution and the absence of detectable impurities. In the ^1H spectrum (**Fig. S5**) the diagnostic signals are δ 10.11 ppm (2H, s, N—H), δ 8.52 ppm (2H, s, C4/C4′), δ 7.65–7.63 ppm (2H, d, J = 8.3 Hz, C2/C2′) plus a multiplet for C3/C3′, and δ 2.14 ppm (12H, s, four CH_3). The ^{13}C spectrum shows a single carbonyl resonance at δ 196.59 ppm (**Fig. S6**). Although FT-IR shows two carbonyl bands, the single ^{13}C signal is consistent with rapid conformational exchange of the carbonyl environments on the NMR timescale. Importantly, H_2L exhibits no vinylic C—H resonance at δ ≈ 5.30 ppm, and the observed N—H shift at δ 10.11 ppm differs from the signals diagnostic of the enaminone tautomer reported by Ahumada et al. (δ 10.87 and 5.36 ppm for N—H and vinylic C—H, respectively) [37]. Together, these data strongly support assignment of H_2L as a non-tautomeric diamine–carbonyl species in solution rather than the enaminone tautomer reported in [37].

Positive-ion ESI mass spectrometry was performed on the free ligand and its coordination complexes (**Fig. S7**). For H_2L, the molecular ion appeared at m/z 329.2 (45 %), consistent with the calculated $(M + H)^+$ for $C_{18}H_{21}N_2O_4$ (329.15 amu). A fragment at m/z 287.2 (11.5 %) most plausibly arises from the loss of an acetaldehyde unit. The peak at 200.0 (30 %) corresponds to a 1-((2E,5Z)-1,4-dihydrobenzob][1,4]diazocin-3-yl)ethen-1-ol fragment. The base peak at m/z 128.2 (100 %) may correspond to one of three possible species; however, structure III is considered the most plausible, owing to the rigidity of the cyclohexane ring and the stabilising effect of the adjacent carbonyl group. The full fragmentation pattern is illustrated in **Scheme S1**.

The spectrum of [Co(L)] (**Fig. S8**) displayed a major peak at m/z 386.2 (100 %), matching the calculated $(M + H)^+$ for $C_{18}H_{19}CoN_2O_4$ (386.1 amu). A secondary signal at 801.4 amu, exhibiting a cobalt-specific isotope pattern, was also observed. This signal does not correspond to a dimer; it is more plausibly attributed to a secondary fragmentation pathway or to a supramolecular species generated during ionisation.

For [Ni(L)] (**Fig. S9**), the molecular ion was recorded at m/z 385.1 (52 %), in agreement with the calculated value for $C_{18}H_{18}NiN_2O_4$. A smaller peak at 329.2 (28 %) may be attributed to the loss of Ni, yielding the free ligand ion. The base peak fragment appeared at 105.1 amu (100 %), assigned to a stable vinylpyridine-type species. No signals attributable to pyrazine or its fragments were detected.

In the case of [Cu(L)]0.5pyrazine (**Fig. S10**), the molecular ion was detected at m/z 389.3 (21 %), consistent with the calculated mass for $C_{18}H_{18}CuN_2O_4$. Although crystallographic analysis indicated a formula weight of 429.94 amu, incorporating 0.5 equivalents of pyrazine, no pyrazine-related signals were observed in the mass spectrum. This

supports the conclusion that pyrazine is present as a lattice molecule rather than a coordinated ligand, and is lost during ionisation due to the absence of bonding to the metal centre. A peak at 252.1 amu may result from the loss of a copper–propylene glycol unit ($C_3H_6CuO_2$, 137 amu). The base peak at *m/z* 137.1 corresponds to a dimethylaminophenol species ($C_8H_{11}NO$; calc. 137.08 amu), which remains stable under MS conditions.

3.4. Electronic spectra and magnetic moment measurement

The electronic spectra of the compounds, measured in DMSO, are summarised in Table 3. The free ligand H_2L showed a broad absorption band at 305 nm, attributed to overlapping $\pi \rightarrow \pi^*$ and $n \rightarrow \pi^*$ transitions [38,39]. At room temperature, the magnetic moments of the paramagnetic Co(II) and Cu(II) complexes were slightly higher than their spin-only values, recorded at 1.75 BM and 1.84 BM, respectively (both S = ½). These slight deviations reflect spin-orbit coupling [40]. The Ni(II) complex gave a value of 0.4 BM (S = 0), consistent with diamagnetic, low-spin behaviour. This minor deviation from zero could be due to trace paramagnetic impurities, subtle variations in ligand field strength, or instrumentation uncertainty, especially considering the ±0.1 BM error margin typical of the Sherwood balance. Comparable magnetic moments have been observed for square planar Ni(II) complexes, generally ranging from 0.4 to 0.8 BM [40].

The low magnetic moment values measured for the Co(II), Cu(II), and Ni(II) compounds (Table 3) align with square planar geometries in the solid state, in agreement with the analytical data and the X-ray structure of the Cu(II) complex. Upon dissolving the complexes in DMSO, each undergoes a clear colour shift to brown, indicating that the solvent interacts directly with the metal centre. This behaviour suggests that DMSO appears to coordinate at the axial positions, causing the coordination environment to expand from square planar to distorted octahedral geometry [36,41].

In contrast to earlier studies where donor solvents such as DMSO were added during complex formation or crystallisation, the present results indicate that the geometry transformation occurs only after the complexes are redissolved in DMSO. The UV–Vis spectral changes support this interpretation, revealing axial coordination of two DMSO molecules accompanied by a shift from square planar to distorted octahedral geometry in solution. Owing to its strong donor capacity and minimal steric hindrance, DMSO effectively stabilises the axial coordination, thereby shifting the square planar–octahedral equilibrium. Comparable solvent-induced transformations have been reported for Co(II) and Cu(II) complexes bearing N_2O_2 donor ligands in coordinating media such as DMF [36]. Ni(II) Schiff-base complexes usually crystallise in square-planar geometries, but when dissolved in DMSO, they tend to bind two axial solvent molecules and adopt an octahedral structure [41a]. This shift has been associated with a spin-state change, resulting in a high-spin octahedral form [41b]. Parallel behaviour has been observed for triazole-based complexes, where DMSO displaces axial chloride ligands, again highlighting the strong influence of coordinating solvents on the final geometry [11]. In contrast to the present study, the replacement of the two chloride ions did not alter the coordination geometry. The effect was instead reflected in the molar conductivity, consistent with the formation of electrolyte species in solution.

3.5. X-ray single-crystal structure of [Cu(L)]·0.5(pyrazine) coordination complex

The X-ray molecular structure with the atom-labelling scheme of complex [Cu(L)]·0.5(pyrazine) is presented in Fig. 1. Crystallographic data are summarised in Table 4, and selected bond lengths, bond angles, and torsion angles are listed in Tables 5–7. The asymmetric unit contains a whole complex of pseudo two-fold symmetry and half of a pyrazine molecule arranged about an inversion centre.

Because no pyrazine was intentionally introduced during synthesis, its presence in the crystal lattice is unexpected. One explanation is the presence of trace pyrazine impurity in the reagents. Alternatively, a Cu(II)-mediated oxidative cyclisation could have generated pyrazine *in situ*. A likely mechanism involves a two-electron redox process that drives decomposition and condensation of amine groups from the ligand or residual *o*-phenylenediamine, followed by dehydrogenation and

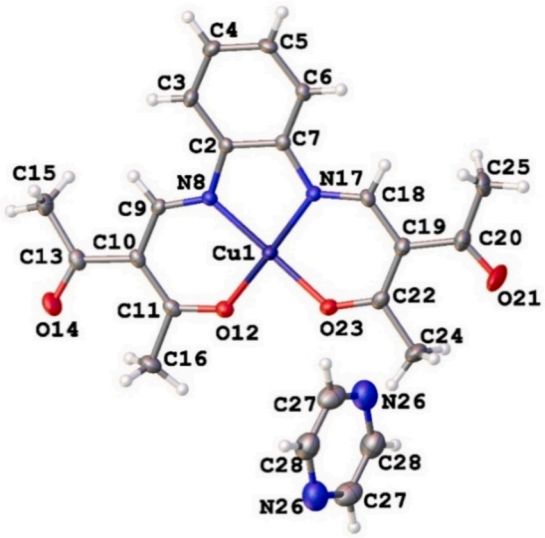

Fig. 1. X-ray molecular structure for [Cu(L)]·0.5(pyrazine) coordination complex.

Table 4
Crystallographic data of [Cu(L)]0.0.5($C_4H_4N_2$) coordination complex.

Parameter	Value
CCDC	2464836
Empirical formula	$C_{20}H_{20}CuN_3O_4$
Formula weight	429.94
Temperature/K	150.4(11)
Crystal system	Monoclinic
Space group	$P2_1/c$
a/Å	11.2732(3)
b/Å	23.5336(5)
c/Å	7.09678(18)
β/°	103.449(2)
Volume/Å^3	1831.14(8)
Z	4
ρcalcg/cm^3	1.560
μ/mm^{-1}	1.226
F(000)	888.0
h, k, l max	12/−14, 32/−23, 9/−9
Theta(max)/°	29.347
Data Completeness	0.888
Tmin, Tmax	0.682, 1.000
Independent Reflections	4467
Reflections [$I \geq 2\sigma$ (I)]	3293
Number of refined parameters (Npar)	257
Goodness-of-Fit (S)	1.046
Final R Indexes [I ≥2σ (I)]	R1 = 0.0456, wR2 = 0.1050

Table 5
Selected bond lengths (Å) in the crystal structure of [Cu(L)]·0.5($C_4H_4N_2$).

Bond distance	Value	Bond distance	Value
Cu1–N8	1.916(2)	Cu1–N17	1.907(2)
Cu1–O12	1.9097(18)	Cu1–O23	1.9089(18)
N8–C2	1.423(3)	N17–C7	1.413(3)
N8–C9	1.309(3)	N17–C18	1.311(3)
C11–O12 (coor.)	1.273(3)	C22–O23 (coor.)	1.279(3)
C13–O14 (uncoor.)	1.224(3)	C20–O21 (uncoor.)	1.208(4)

Table 6
Selected bond angles (°) in the crystal structure of [Cu(L)]·0.5($C_4H_4N_2$).

Bond angle	Value	Bond angle	Value
O12–Cu1–N8	92.33(8)	N17–Cu1–O12	177.36(9)
O23–Cu1–N8	174.11(9)	N17–Cu1–O23	92.38(8)
O23–Cu1–O12	89.72(8)	N17–Cu1–N8	85.73(9)
C11–O12–Cu1	129.84(17)	C22–O23–Cu1	129.71(17)
C2–N8–Cu1	111.92(16)	C7–N17–Cu1	112.62(16)
C9–N8–Cu1	125.46(18)	C18–N17–Cu1	124.75(18)
C9–N8–C2	122.6(2)	C18–N17–C7	122.6(2)
C7–C2–N8	114.8(2)	C2–C7–N17	114.8(2)
C3–C2–N8	125.5(2)	C6–C7–N17	125.9(2)

Table 7
Selected torsion angles (°) in the crystal structure of [Cu(L)]·0.5($C_4H_4N_2$).

Torsion angle	Value	Torsion angle	Value
Cu1–N8–C2–C7	2.4(3)	Cu1–N17–C7–C2	1.1(3)
Cu1–N8–C9–C10	2.4(4)	Cu1–N17–C18–C19	−4.3(4)
Cu1–O12–C11–C10	7.1(4)	Cu1–O23–C22–C19	5.2(4)
Cu1–O12–C11–C16	−172.78(18)	Cu1–O23–C22–C24	−174.37(19)

cyclisation. Such a pathway resembles the oxidative cyclisation of 1,2-diamines under Cu(II)-mediated heating conditions [42]. Although direct mechanistic proof is unavailable, the crystallographic evidence is consistent with this pathway.

The [Cu(L)]·0.5(pyrazine) complex crystallises in the monoclinic crystal system, space group $P2_1/c$. The Cu(II) ion is chelated by the N_2O_2 donor set of the ligand in a nearly square-planar geometry, as confirmed by the coordination bond angles (Table 5). The complex has almost coplanar atoms, and the most deviating from the mean plane are C15 (+0.34 Å), O14 (−0.23 Å) and C24 (−0.22 Å).

The τ_4 parameter (calculated as 360-(α + β)/141, where α and β are the larger coordination bond angles) is ≈ 0.06, supporting a slightly distorted square-planar geometry. This analysis follows the method originally defined by Yang et al. [43a], in analogy to the τ_5 index of Addison et al. [43b], who noted that τ_4 provides an objective complement to visual inspection. For a recent overview of geometry indices, see the treatment by Guchhait et al. [43c]. Due to ligand-field stabilisation, the d^9 electron configuration of Cu(II) favours square-planar geometry or square pyramidal. Jahn–Teller distortion may lead to axial bond elongation, resulting in a square-pyramidal or octahedral geometry. In solution, the geometry may expand to a square-pyramidal or octahedral geometry through the coordination of solvent molecules.

The coordination bond lengths are Cu1–N8 = 1.916(2) Å, Cu1–N17 = 1.907(2) Å, Cu1–O12 = 1.910(2) Å, and Cu1–O23 = 1.909(18) Å. These values fall within the expected range for typical square-planar Cu(II) complexes with deprotonated amine ligands.

The X-ray data show that the C═O bonds of coordinated oxygens (C11–O12 = 1.273(3) Å and C22–O23 = 1.279(3) Å) are slightly longer than the uncoordinated C═O bonds (C13–O14 = 1.224(3) Å and C20–O21 = 1.208(4) Å). The mean elongation is ≈ 0.06 Å (≈ 5 %) relative to uncoordinated C═O bonds (1.208–1.224 Å), which are consistent with typical C═O bond lengths of 1.20–1.23 Å reported for uncoordinated carbonyl groups in organic molecules [44a]. This aligns with previous crystallographic findings for N_2O_2 Schiff-base-type Cu(II) complexes [37]. This trend reflects partial back-donation from the filled Cu(II) $3d_{x^2-y^2}$ orbital into the π* orbitals of the carbonyl group, reducing the C═O bond order and slightly increasing its length. The parallel FT-IR downshift of the carbonyl stretching band ($\Delta\nu$ = 16–27 cm^{-1}; mean ≈ 21 cm^{-1}) and HOMO electron density localisation at the Cu—O moiety (from DFT) both corroborate this interpretation.

Such metal-to-ligand electron delocalisation enhances covalent character in the Cu—O interaction, influencing both stability and catalytic potential. The resulting redistribution of charge within the coordination plane rationalises the experimentally observed spectroscopic features and the moderate energy gap determined by DFT.

Although the free ligand is diamine in nature, as confirmed by NMR and FTIR spectra, coordination to Cu(II) induces deprotonation and electron redistribution, giving the nitrogen donors partial imine-like (C=N) character in the complex, consistent with the observed shortening of C—N bond distances in the X-ray structure. Thus, while the precursor ligand is not a Schiff base, the coordinated nitrogens are most appropriately described as imine-type donors within a deprotonated N_2O_2 framework [37]. Comparable Cu(II)–N_2O_2 diamine complexes reported in the literature exhibit closely related structural features. For example, a study [44b] reports a square-planar *trans*-N_2O_2 Cu(II) complex with Cu–N/O distances of ~1.91 Å. While another study [44c] shows near-planar arrangements in a related diamine–phenolic scaffold. Although these precedents are based on diamine ligands rather than Schiff bases, their bond lengths and geometries reinforce the assignment of imine-type donors within the deprotonated N_2O_2 framework of the present complex.

Beyond the solid-state structural features, electronic structure calculations provide further insight. The smaller HOMO-LUMO gap (ΔE = 3.9110 eV) is expected to promote catalytic activity by facilitating electron transfer in redox cycling. In addition, DFT calculations indicate a moderate dipole moment (DM = 2.8839 D), a property that may favour electron delocalisation within the system. This feature modulates the stability of intermediate states and supports effective interactions between reagents during catalysis. The high polarisability (α = 305.2713 a.u.), hyperpolarisability (β = 22,033.70 a.u.), and softness (S = 0.5113) further demonstrate the strong electronic adaptability of the system and enhanced nonlinear optical response. Overall, these global descriptors suggest that the system may participate in oxidative processes. The square-planar geometry of the Cu(II) complex may also provide a template effect that facilitates assembly of pyrazine from residues generated during ligand decomposition, under the employed reaction conditions.

3.6. DFT modelling

The quantum chemical calculations were performed for four compounds using the GAUSSIAN 16, revision A.03 [33]. Geometry optimisations and electronic structure analyses were performed at the DFT/B3LYP level of theory. The LANL2DZ basis set with effective core potential was applied for coordination complexes, while the 6–311 + G(d, p) for the ligand [34,4]. Calculations were performed on the Pentium (R) 4/IPM-PC with a 3.00 GHz CPU and 2.00 GB RAM. The optimised geometries and orbital analyses formed the basis for subsequent MEP and NLO investigations.

3.6.1. Geometry optimisation

The structurally optimised geometries of the ligand (H_2L) and its coordination complexes with Co(II), Ni(II) and Co(II) are visualised in Fig. 2. The ligand H_2L incorporates diamine and dicarbonyl donor atoms, forming a N_2O_4 tetradentate chelating system. In each of the three neutral coordination complexes, the metal is surrounded by a square-planar coordination environment. These optimised structures are consistent with the experimental spectroscopic and magnetic data, confirming the reliability of the computational approach.

3.6.2. Frontier molecular orbital analysis

The electronic distributions of the HOMO and LUMO were examined to explore the local reactivity of H_2L and its metal coordination complexes with Co(II), Ni(II), and Cu(II) (see Fig. 3) [4,5,34,35]. For the free ligand, the HOMO is largely delocalised over the phenyl ring and other conjugated π-regions, making these areas electron-rich and susceptible to electrophilic attack. The LUMO, in contrast, tends to settle over the carbonyl groups on the right-hand side of the molecule, as well as across sections of the *o*-phenylenediamine core. These areas, being rich in electron-withdrawing characteristics, help stabilise the LUMO and make the molecule receptive to nucleophilic attack. When the ligand

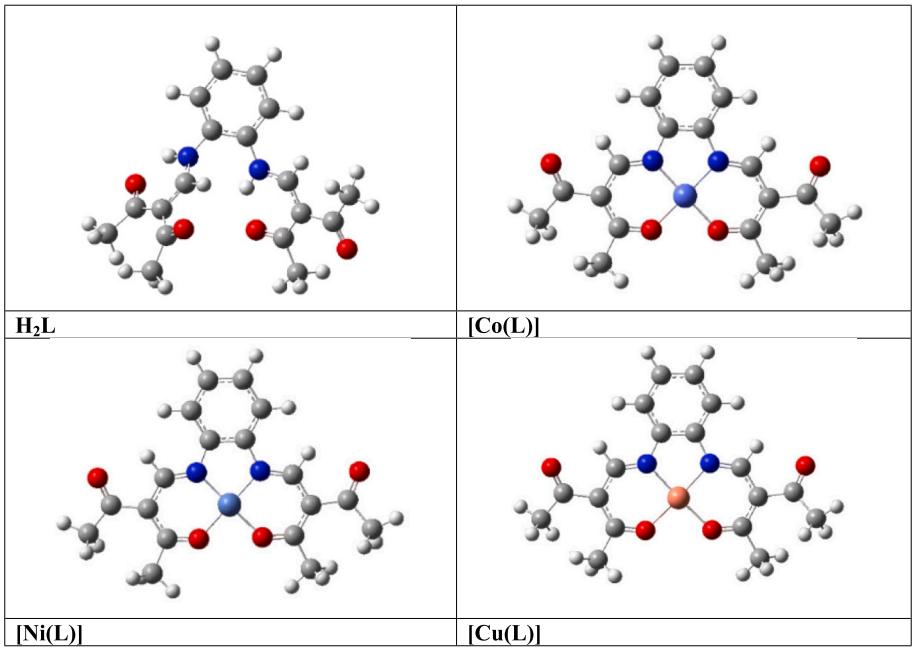

Fig. 2. The 3-D optimised geometry of H_2L, [Co(L)], [Ni(L)], and [Cu(L)] coordination complexes.

coordinates with the metal, the HOMO spreads consistently across the aromatic rings and coordinated carbonyl groups, with electron density extending toward the metal centre. This reflects good orbital overlap and sharing between the metal and ligand. The LUMO, on the other hand, shifts more noticeably, becoming concentrated on the metal's d-orbitals, supported by the ligand's π-system. This redistribution leaves the metal centre slightly electron-deficient, making it more open to interactions with donor molecules such as coordinating solvents. In contrast to conventional Schiff-base N_2O_2 frameworks, in which the frontier orbital density is predominantly localised on the imine donor sites, the diamine-derived scaffold facilitates extended electronic delocalisation encompassing both the aromatic backbone and the coordinated metal centre. This electronic distribution enhances charge-transfer pathways and thereby provides a mechanistic rationale for the pronounced nonlinear optical (NLO) response observed experimentally.

3.6.3. *Global reactivity descriptors*

To gain clearer insight into the electronic behaviour of the studied compounds, several chemical global reactivity descriptors (CGRDs) were calculated using DFT. These included the energies of the HOMO and LUMO orbitals, the energy gap (ΔE), chemical hardness, softness, and other factors related to stability and reactivity (see Table 8) [4,5,34,35]. The HOMO, or highest occupied molecular orbital, represents how easily a molecule can give away electrons, while the LUMO, the lowest unoccupied orbital, shows how ready it is to receive them [4,5,34]. Looking at where these orbitals sit energetically gives a good sense of how electronically rich or poor each compound is. Based on the HOMO energy levels, the compounds become progressively better at donating electrons in the order: ligand < cobalt < copper < nickel. The LUMO energies follow a similar pattern, with nickel at the highest and the ligand at the lowest. Generally, when the energy gap (ΔE) between these orbitals is smaller, the molecule tends to be more chemically reactive but less stable in terms of kinetic resistance [45]. Among the complexes studied, the copper species shows the narrowest energy gap, which suggests it's the softest, electronically speaking, and most likely to take part in charge-transfer processes [14,28].

This is also reflected in its electrical conductivity and catalytic behaviour, and it also underpins its superior NLO performance. The combination of a narrow ΔE, extended delocalisation, and diamine-based stability directly addresses the limitations of Schiff base frameworks. These features demonstrate that the present system is both robust and electronically versatile, providing a distinctive N_2O_2 platform. Fig. 4 provides a clear visual of how the ΔE values compare across the compounds.

The ligand possesses the largest energy gap, which generally reflects greater structural stability and a limited tendency to engage in chemical reactions. In contrast, the copper complex shows a markedly narrower gap, pointing to increased electrical conductivity and a higher level of chemical reactivity. This kind of trend fits with Eq. 1, where conductivity (σ) is tied directly to the energy gap:

$$\sigma \propto \exp.(-\Delta E / kT) \quad (1)$$

where k is the Boltzmann constant and T is the temperature [4,5,12,15].

Chemical hardness, calculated as $\eta = 0.5(ELUMO - EHOMO)$, measures how resistant a molecule is to changing its electronic structure [4,5]. The order of decreasing hardness is: ligand > nickel > cobalt > copper. Softness, the inverse ($S = 1/\eta$), follows the opposite pattern, meaning copper is the softest and most electronically flexible [4,5]. What's particularly striking is how these computed properties reflect the actual chemical behaviour. The Cu(II) complex seems to owe its catalytic behaviour to both its softness and low energy gap (ΔE), particularly its ability to decompose the ligand under reducing conditions to form a pyrazine derivative [42]. Interestingly, these same electronic features also appear to enhance its nonlinear optical response, making the Cu(II) complex a promising candidate for both catalytic and optical applications [27,28].

3.6.4. *Molecular electrostatic potential (MEP)*

The electron density distribution was analysed using the molecular electrostatic potential (MEP) approach, which helps identify the most likely regions for electrophilic and nucleophilic attack, as well as potential hydrogen bonding interactions (see Fig. 5).

In H_2L, the aromatic rings and associated π-electron domains, which correspond to the principal localisation of the HOMO, constitute the most reactive sites toward electrophilic attack. Red regions on the MEP surface mark the electron-rich domains consistent with the HOMO localisation. In contrast, the LUMO is predominantly localised over electron-deficient regions, particularly around the carbonyl groups.

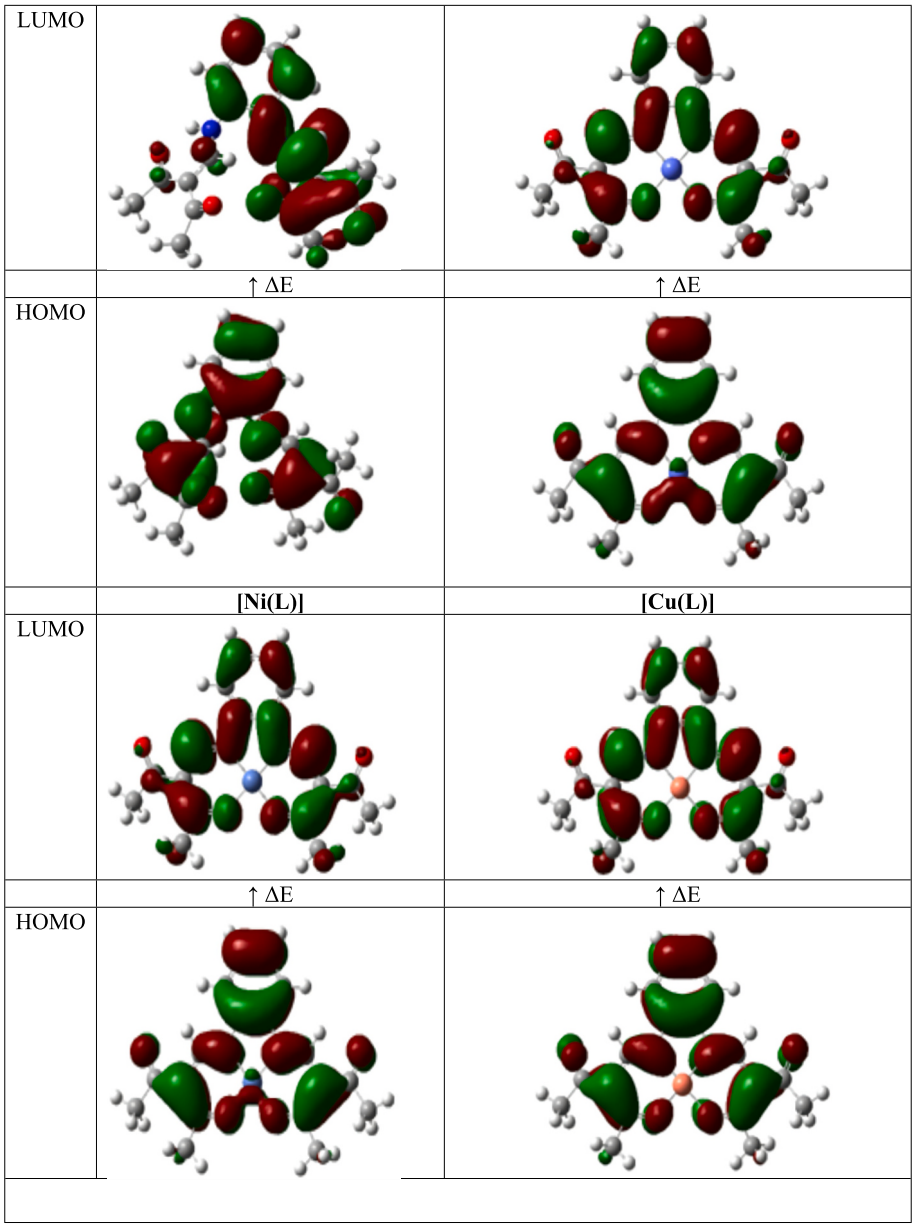

Fig. 3. The HOMO–LUMO computed map of the examined compounds derived from DFT calculations.

Table 8
DFT simulation parameters for H_2L, coordination complexes and reference materials.

Parameter	H_2L	Ni(II)	Co(II)	Cu(II)	Urea	pNA	MNA
α (a.u.)	270.9033	282.0353	304.4410	305.2713	328.9466	114.6110	103.8334
β (a.u.)	1141.1871	8236.09518	3022.78687	22,033.699	47.9164	2052.8823	2075.6464
S	0.4744	0.5024	0.5028	0.5113	–	–	–
η	2.1077	1.9903	1.9887	1.9555	–	–	–
E_{GAP} (eV)	4.2155	3.9807	3.9774	3.9110	–	–	–
LUMO (eV)	−2.1771	−1.9518	−2.1246	−2.1328	–	–	–
HOMO (eV)	−6.3927	−5.0439	−6.1021	−6.0439	–	–	–
D.M (μ)	4.5266	2.9318	2.8425	2.8839	–	–	–

These appear as blue domains in the MEP surface, marking them as the most favourable sites for nucleophilic attack.

In these coordination complexes, the HOMO extends over both the aromatic framework and the coordinated carbonyl ligands, reflecting orbital overlap between the ligand and the metal centre. This delocalisation is reflected by red regions in the corresponding MEP maps. The calculated ΔE values are consistent with the MEP visualisations, as smaller energy gaps correspond to greater charge separation and enhanced charge mobility, most pronounced in the Cu(II) complex. This property is a key contributor to nonlinear optical (NLO) behaviour.

The MEP surface values span −0.005266 to +0.005266 a.u. for the free ligand (H_2L) and − 0.005154 to +0.005154 a.u. (Ni), −0.005189 to

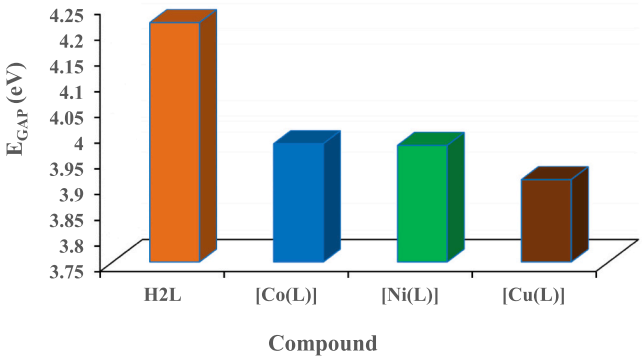

Fig. 4. Calculated the ΔE (HOMO-LUMO) gap values for the ligand and its coordination complexes.

+0.005189 a.u. (Cu), and − 0.005102 to +0.005102 a.u. (Co) for these complexes. These results show that coordination to the metal centre influences the surface charge distribution. Conversely, the most electropositive regions (depicted in blue) are favourable sites for nucleophilic interactions, as illustrated in Fig. 5 [47]. Importantly, the Cu(II) complex combines a narrow ΔE with extended HOMO delocalisation, features that favour intramolecular charge transfer and underpin its strong nonlinear optical response, discussed in the following section.

3.6.5. Nonlinear optical properties

3.6.5.1. Computational evaluation of β and α. The first hyperpolarisability (β), a principal measure of second-order susceptibility, was determined at the B3LYP/6–311 + G(d,p) level for H_2L and with the LANL2DZ basis set for the coordination complexes. This quantity describes how the molecular dipole moment responds to an external electric field [46a]. As hyperpolarisability is strongly influenced by intramolecular charge transfer (ICT), it provides a direct indication of a compound's nonlinear optical (NLO) behaviour [46b]. All studied compounds exhibited higher α and β values than the reference standards urea, *p*-nitroaniline (pNA), and 2-methyl-4-nitroaniline (MNA), indicating enhanced NLO activity. The β values follow the trend: Cu > Ni > Co > MNA > pNA > ligand > urea (see Fig. 6), showing that the copper complex has the strongest response.

The polarisability (α) values, obtained at the same computational level, were also higher than those of pNA and MNA. The α values obtained for [Co(L)] and [Cu(L)] agreed well with those of urea, confirming that the computational method is reliable [48]. As summarised in Table 8, these two complexes combine low ΔE, high α, and moderate dipole moment, features consistent with adaptable electronic structures. Although the dipole moments are moderate, their flexibility favours

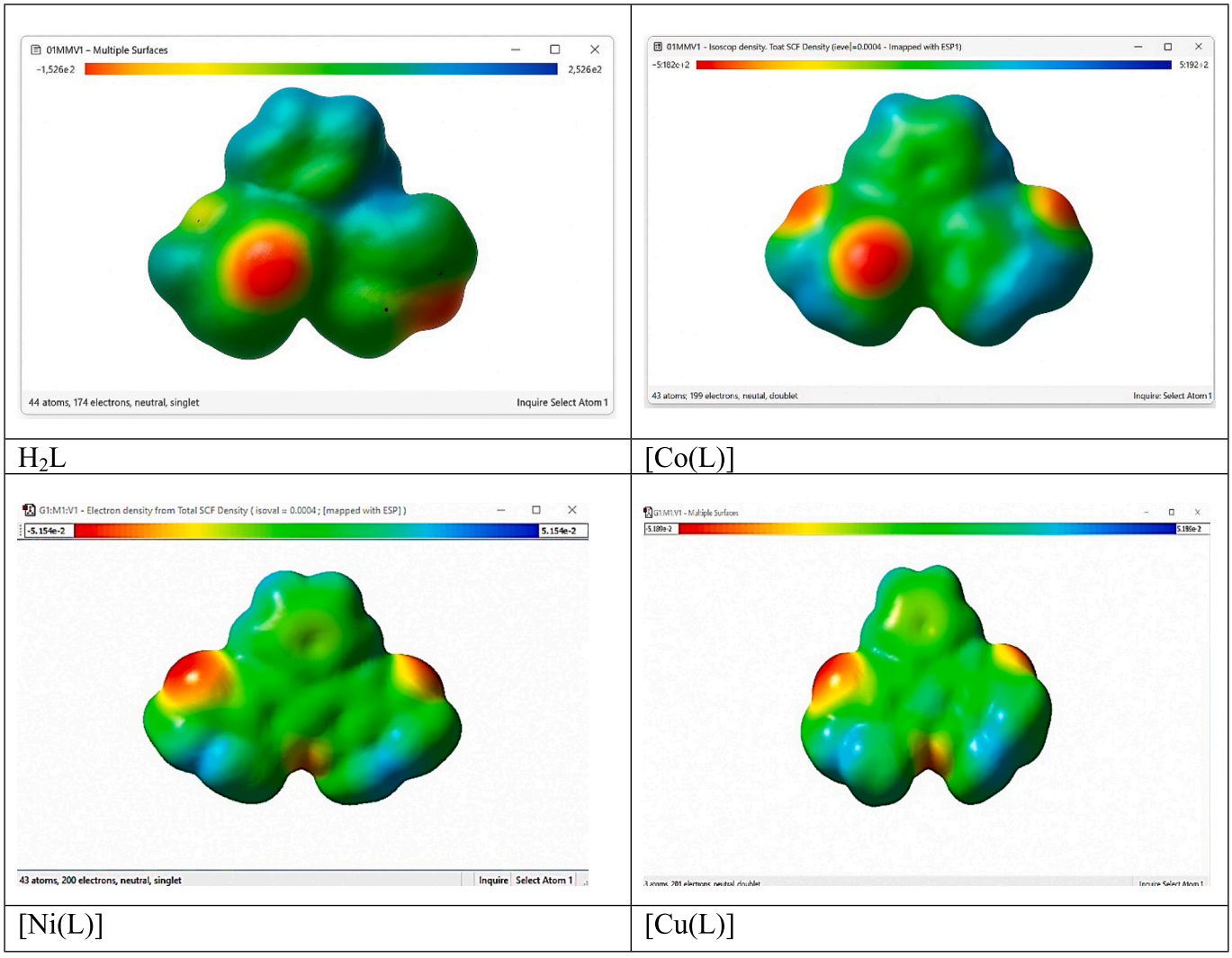

Fig. 5. Molecular electrostatic potential (MEP) distribution map of H_2L at the DFT/B3LYP/6–311 + G(d,p) level and its coordination complexes at the LANL2DZ level.

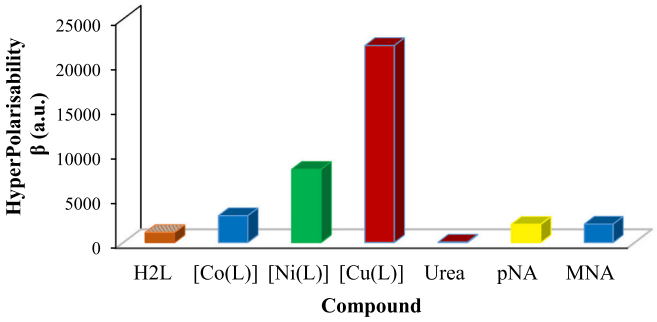

Fig. 6. Comparison of hyperpolarisability (β) values for H_2L, coordination complexes, and reference materials.

charge delocalisation and efficient ICT. Since α underpins the NLO response, the evaluation of higher-order properties such as third-order hyperpolarisability (γ) is relevant for a fuller picture [49]. Previous work [28] reported γ values of 444 × 10^{-36} esu for Ni(II) and 567 × 10^{-36} esu for Cu(II), distinct from the β values considered here. The present study, therefore, focuses on the static hyperpolarisability (β), the key descriptor of second-order NLO behaviour.

3.6.5.2. Mechanistic origin of the NLO response. The strong nonlinear optical response of the Cu(II) complex arises from the interplay between its solvent-driven geometrical change and the accompanying redistribution of electron density. In the solid-state, the complex is nearly square-planar, whereas in DMSO, axial coordination of solvent molecules expands the sphere toward a distorted octahedral geometry. This adjustment increases orbital overlap and stabilises the electronic configuration.

DFT calculations reveal that the HOMO is delocalised across the aromatic backbone, carbonyl donors, and the Cu(II) centre, providing an effective path for intramolecular charge transfer. The small HOMO–LUMO gap (ΔE = 3.911 eV) and high global softness (S = 0.5113) indicate an electronically pliable system capable of strong polarisation. The slight elongation of the Cu—O and Cu—N bonds suggests redistribution of electron density within the coordination sphere, which in turn influences dipole behaviour.

Altogether, these factors explain the large β value for the Cu(II) complex (2.20 × 10^4 a.u.; ≈ 190 × 10^{-30} esu), which is more than 50 % higher than typical for related Cu(II) chromophores. The coupling of geometry switching, orbital delocalisation, and solvent-assisted stabilisation thus provides a consistent mechanistic rationale for the pronounced second-order NLO behaviour in this diamine-derived N_2O_2 system.

3.6.5.3. Comparative analysis with reported systems. The diamine-derived N_2O_2 framework presented here, which may be regarded as a partial imine-type system, shows a markedly stronger second-order NLO response than most reported Cu(II) and Ni(II) analogues. The Cu(II) complex yields β = 2.20 × 10^4 a.u. (≈ 190 × 10^{-30} esu), and the Ni(II) analogue β = 8.82 × 10^3 a.u. (76.2 × 10^{-30} esu), placing both near the upper range of known Schiff-base derivatives. Mohan et al. [28] reported Cu(II) Schiff-base complexes with third-order hyperpolarisabilities (γ = 5.67 × 10^{-34} esu), corresponding to higher-order effects rather than the second-order properties considered here. Manurkar et al. [29a] obtained β ≈ 1.4 × 10^4 a.u. (≈ 121 × 10^{-30} esu) for glutamine-derived Cu(II) systems, while Abd El-Nasser and Ismail [50] found β ≈ 8.2 × 10^3 a.u. (≈ 71 × 10^{-30} esu) for a benzothiazole-amide Cu(II) complex, indicating that certain non-Schiff-base species can also exhibit measurable NLO activity.

Comparable results have been observed in other systems, as summarised in Table 9. Chiral Cu(II) Schiff-base complexes generally fall within β = (2.5–5.7) × 10^3 a.u. (22–49 × 10^{-30} esu) [51a]; unsymmetrical Ni(II) analogues yield β = (4.9–12.5) × 10^3 a.u. (42–108 × 10^{-30} esu) [51b]; and Wittig-based ligands reach β ≈ 8.1 × 10^3 a.u. (≈ 6.97 × 10^{-30} esu) [52]. By contrast, the diamine complexes described in this work surpass these benchmarks while retaining superior hydrolytic stability. Notably, an isolated high-performance case, the ferrocenyl-carboxylate Cu(II) Schiff-base complex (β = 2.78 × 10^4 a.u.; 240 × 10^{-30} esu) [56], achieves similar values; nonetheless, the present diamine N_2O_2 compounds demonstrate comparable NLO strength together with improved robustness and lower symmetry.

In summary, the diamine-based complexes perform as well as, or better than, comparable Schiff-base systems while offering enhanced hydrolytic stability and solvent-responsive adaptability. These findings suggest that this framework provides a reliable basis for the design of next-generation second-order NLO materials.

4. Conclusions

The coordination behaviour of the ligand provides valuable insights into the design of N_2O_2-based nonlinear optical (NLO) materials. We synthesised a tetradentate diamine ligand, 3,3′-((1,2-phenylenebis(azanediyl))bis(methanylylidene))-bis(pentane-2,4-dione), and its Co(II), Ni(II) and Cu(II) complexes, in which the ligand acts as a dibasic N_2O_2 donor. Spectroscopic and analytical data confirmed near square-planar geometries in the solid state, supported by single-crystal X-ray analysis of [Cu(L)]·0.5(pyrazine). In the DMSO solution, reversible axial coordination of two solvent molecules converts the complexes into octahedral species.

DFT calculations reproduced the observed structural transformations for all complexes, yielded global reactivity descriptors, and revealed π-back bonding through C═O bond elongation and HOMO delocalisation over the metal–ligand framework. For the Cu(II) complex specifically, the smallest HOMO–LUMO gap (ΔE = 3.911 eV) was observed, along with the highest polarisability (α = 305.3 a.u.) and an exceptionally large hyperpolarisability (β = 2.20 × 10^4 a.u.), surpassing pNA, MNA and urea, thereby confirming a pronounced second-order NLO response.

The X-ray data also show that although the free ligand is diamine in nature, coordination to Cu(II) induces deprotonation and electron redistribution. The nitrogen donors thereby acquire imine-like character. This transformation integrates the hydrolytic stability of diamines with the electronic properties of Schiff bases, emphasising the relevance of these complexes within the broader N_2O_2 family.

The diamine-based N_2O_2 scaffold exhibits remarkable hydrolytic stability, solvent-responsive modulation of geometry, and enhanced nonlinear optical performance. MEP mapping validates the electronic redistribution inferred from DFT calculations and delineates the charge-transfer channels underlying the strong optical response. The presence of pyrazine in the Cu(II) crystal lattice further indicates a Cu(II)-mediated cyclisation process, consistent with its catalytic activity.

This unique combination of hydrolytic stability, structural adaptability, and strong NLO performance addresses a long-standing gap in diamine-derived N_2O_2 ligand chemistry and establishes a robust, tunable platform for the development of next-generation dynamic photonic, optoelectronic, and redox-related materials.

CRediT authorship contribution statement

Jasim M.S. Alshawi: Writing – review & editing, Validation, Methodology, Formal analysis, Data curation, Conceptualization. **Baidaa K. Al-Rubaye:** Visualization, Methodology, Data curation, Conceptualization. **Hanadi M. Jarallah:** Writing – original draft, Visualization, Formal analysis, Data curation. **Sadiq M.-H. Ismael:** Writing – original draft, Validation, Software, Data curation, Conceptualization. **Mohamad J. Al-Jeboori:** Writing – review & editing, Writing – original draft, Validation, Supervision, Software, Project administration, Conceptualization. **Inigo J. Vitorica-Yrezabal:** Writing

Table 9
Comparative β values and computational levels for Cu(II) and Ni(II) complexes from this work and selected literature.

System	β (a.u.)	β ($\times 10^{-30}$ esu)	Method/level of theory	Reference
Cu(II), diamine N_2O_2 (partial imine-like)	2.20×10^4	≈ 190	DFT (B3LYP/LANL2DZ)	This work
Ni(II), diamine N_2O_2 (partial imine-like)	8.82×10^3	76.2	DFT (B3LYP/LANL2DZ)	This work
Glutamine–Cu(II)	1.4×10^4	≈ 121	B3LYP/6-31G(d,p) + LANL2DZ	[29a]
Benzothiazole-amide–Cu(II)	8.2×10^3	≈ 71	B3LYP/6-31G(d,p) + LANL2DZ	[50]
Chiral Cu(II)–Schiff base	$(2.5–5.7) \times 10^3$	(22–49)	CAM-B3LYP/6–311++G(d,p)	[51a]
Ni(II)–unsym. Schiff base	$(4.9–12.5) \times 10^3$	(42–108)	CAM-B3LYP/6–311++G(d,p), EFISH	[51b]
Wittig Schiff ligands	up to 8.1×10^3	up to 6.97	B3LYP/6-31G + LANL2DZ	[52]
Cu(II), naphthyl-imine N_2O_2	≈ 7890	6817	FF (UHF/LanL2mb)	[53]
Triphenolic Schiff base macrocycle	≈ 818	7.066	Semi-empirical (AM1)	[54]
Organometallic Cu(II) Schiff base	≈ 818	7.066	Semi-empirical (AM1)	[55]
Ferrocenyl–carboxylate Cu(II) Schiff base	2.78×10^4	240	Experimental (HLS, λ = 1.91	[56]

Conversion note: 1 a.u. = 8.6393×10^{-33} esu (for β).

– original draft, Visualization, Software, Data curation. **Richard E.P. Winpenny:** Writing – original draft, Supervision, Resources, Conceptualization.

Author statement

We confirm that all authors have contributed significantly to the conception, synthesis, spectroscopic and crystallographic analysis, DFT calculations, and manuscript preparation. All authors have read and approved the final version of the manuscript. This work is original, has not been published previously, and is not under consideration elsewhere. The authors declare no conflicts of interest. Crystallographic data (CIF files), and spectroscopic data are provided as Supplementary Information to ensure reproducibility and transparency.

Declaration of competing interest

The authors declare that they have no known competing financial interests or personal relationships that could have appeared to influence the work reported in this paper.

Acknowledgements

The authors gratefully acknowledge the support of the Iraqi Ministry of Higher Education and Scientific Research; the Department of Chemistry, College of Education for Pure Science (Ibn Al-Haitham), University of Baghdad; and the Department of Chemistry, College of Education for Pure Science, University of Basrah, for providing laboratory facilities.

Appendix A. Supplementary data

Supplementary data to this article can be found online at https://doi.org/10.1016/j.inoche.2025.115873.

Data availability

Data will be made available on request.

References

[1] Y. Zhang, P. Müller, Recent advances in ligand Design for Transition Metal Catalysis, Coord. Chem. Rev. 512 (2024) 214–256, https://doi.org/10.1016/j.ccr.2024.214256.
[2] M.T. Rees, A.K. Gupta, Emerging synthetic strategies in coordination-driven self-assembly, Chem. Soc. Rev. 53 (2024) 1123–1164, https://doi.org/10.1039/D3CS00876A.
[3] R. Singh, H. Yamamoto, Coordination Complexes in Sustainable Industrial Applications: A 2025 Perspective, Coord. Chem. Rev. 528, (2025) 1–48. Doi: https://doi.org/10.1016/j.ccr.2025.001048.
[4] M.A. Hameed, M.J. Al-Jeboori, Synthesis, spectral characterisation, DFT calculations, biological evaluation and molecular docking analysis of new Mannich compounds derived from cyclopentanone, J. Mol. Struct. 1322 (2025) 140619.
[5] M.A. Hameed, M.J. Al-Jeboori, Dual inhibitory potential and comprehensive investigation of a bis-semi-carbazone ligand: a comparative study with its precursor, Adv. J. Chem. A 8 (5) (2025) 913–929, https://doi.org/10.48309/AJCA.2025.480289.1694.
[6] B.K. Al-Rubaye, M.J. Al-Jeboori, H. Potgieter, Metal complexes of multidentate N_2S_2 heterocyclic Schiff-base ligands; formation, structural characterisation and biological activity, J. Phys. Conf. Ser. 1879 (2021) 022074, https://doi.org/10.1088/1742-6596/1879/2/022074.
[7] N.J. Hussien, J.M.S. Alshawi, K.T. Abdullah, E.I. Yousif, M.J. Al-Jeboori, Dimethyltin(IV) complexes of new thiosemicarbazone ligand with piperazine-1-ylmethylene moiety: synthesis, spectral characterisation and antibacterial activity, Edelweiss Appl. Sci. Technol. 9 (3) (2025) 266–278.
[8] X. Zhou, L. Pang, G. Nie, X. Huang, W. Peng, Y. Xu, Y. Lin, Z. Wu, D. Zhao, Y. Zhu, Successive modification of polydentate complexes gives access to planar carbon- and nitrogen-based ligands, Nat. Commun. 10 (2019) 1742, https://doi.org/10.1038/s41467-019-09367-8.
[9] D.J. Abaas, M.J. Al-Jeboori, Coordination compounds of carbonyl oxygen polychelate ligand; synthesis, physicochemical characterization and biological evaluation, Rev. Bionatura 8 (2) (2023) 18.
[10] S.A. Hussain, M.J. Al-Jeboori, New metal complexes derived from Mannich-base ligand; synthesis, spectral characterisation and biological activity, J. Glob. Pharm. Technol. 11 (2) (2019) 548–560.
[11] (a)Conradie, M.M. Conradie, Z. Mtshali, D. van der Westhuizen, K.M. Tawfiq, M.J. Al-Jeboori, S.J. Coles, C. Wilson, J.H. Potgieter, Synthesis, characterisation and electrochemistry of eight Fe coordination compounds containing substituted 2-(1-(4-R-phenyl-1H-1,2,3-triazol-4-yl)pyridine ligands, R = CH_3, OCH_3, COOH, F, Cl, CN, H and CF_3, *Inorg. Chim. Acta* 484 (2019) 375–385, (b) Conradie, M.M. Conradie, K. Tawfiq, M.J. Al-Jeboori, S.J. Coles, C. Wilson, H.J. Potgieter, Novel dichloro(bis{2-[1-(4-methylphenyl)-1H-1,2,3-triazol-4-yl-κN_3]pyridine-κN})metal (II) coordination compounds of seven transition metals (Mn, Fe, Co, Ni, Cu, Zn and Cd), *Polyhedron* 151 (2018) 243–254.
[12] M.H. Ali, A.A. Al-Shemary, R.M. El-Ferjani, Synthesis, crystal structure and DFT study of a new N_2O_2 donor Schiff base ligand and its co(III) complex, J. Mol. Struct. 1275 (2023) 134752, https://doi.org/10.1016/j.molstruc.2023.134752.
[13] S. Saha, A. Ghosh, Chelation-assisted stabilization of transition metal complexes: a thermodynamic and structural perspective, Coord. Chem. Rev. 478 (2023) 214964, https://doi.org/10.1016/j.ccr.2023.214964.
[14] B.I. Ceylan, Q. Poladian, O. Bölükbaşi-Yalçınkaya, B. Türkmenoğlu, Y. Kurt, N_2O_2 tetradentate Schiff-base Ni(II) and Fe(III) complexes derived from 2-hydroxy-5-ethoxyacetophenone S-methylthiosemicarbazone: synthesis, characterisation, DFT calculations, molecular docking, and antioxidant activity, SSRN Preprint (2025), https://doi.org/10.2139/ssrn.5180212.
[15] S.R. Trifunović, V.D. Miletić, V.V. Jevtić, A. Meetsma, Z.D. Matović, Nickel(II) in chelate N_2O_2 environment: DFT approach and in-depth molecular orbital and configurational analysis, Dalton Trans. 42 (2013) 13262–13274, https://doi.org/10.1039/C3DT51099A.
[16] (a) S.N. Shtykov, Coordination compounds (chelates) in analytical chemistry: solutions, sorbents, and Nanoplatforms, Russ. J. Coord. Chem. 48 (2022) 622–630, https://doi.org/10.1134/S1070328422100062;
(b) J.M.S. Alshawi, M.Q. Mohammed, H.F. Alesary, H.K. Ismail, S. Barton, Voltammetric determination of Hg^{2+}, Zn^{2+}, and Pb^{2+} ions using a PEDOT/NTA-modified electrode, ACS Omega 7 (2022) 20405–20419, https://doi.org/10.1021/acsomega.2c02682.
[17] (a)P.K. Omer, N.M. Aziz, R.A. Omer, Comprehensive review of metal-based coordination compounds in cancer therapy: from design to biochemical reactivity, *Rev. Inorg. Chem.* 44 (4) (2024) 699–710. Doi: https://doi.org/10.1515/revic-2024-0030, (b) T. H. Mawat, M.J. Al-Jeboori, Synthesis, characterisation, thermal properties and biological activity of coordination compounds of novel selenosemicarbazone ligands, *J. Mol. Struct.* 1208 (2020) 127867. Doi: https://doi.org/10.1016/j.molstruc.2020.127876.
[18] J. Malinowski, D. Zych, D. Jacewicz, B. Gawdzik, J. Drzeżdżon, Application of coordination compounds with transition metal ions in the chemical industry—a review, Int. J. Mol. Sci. 21 (15) (2020) 5443, https://doi.org/10.3390/ijms21155443.
[19] S.N. Mahendran, R. Prabhaharan, A. Gurusamy, P. Prasanthrajan, C. Chandrakumar, Y. Yuvaraj, Amino acid-chelated micronutrients: a new frontier in crop nutrition and abiotic stress mitigation, Plant Sci. Today 11 (2024) 8302, https://doi.org/10.14719/pst.8302.

[20] J. Singh, R.J. Staples, J.M. Shreeve, Coordination-driven safer and sustainable energetic materials, J. Mater. Chem. A 13 (2025) 11475–11485, https://doi.org/10.1039/D5TA01130B.

[21] W. Bauer, B. Ossiander, B. Weber, Synthesis of iron(II) complexes with asymmetric N_2O_2 coordinating Schiff base-like ligands and their spin crossover properties, Front. Chem. Sci. Eng. 12 (2018) 400–408, https://doi.org/10.1007/s11705-018-1753-4.

[22] S.M. Abd El-Hamid, S.A. Sadeek, S.F. Mohammed, F.M. Ahmed, M.S. El-Gedamy, N_2O_2-chelate metal complexes with Schiff base ligand: synthesis, characterisation and contribution as a promising antiviral agent against human cytomegalovirus, Appl. Organomet. Chem. 37 (2023) e6958.

[23] W. Su, S. Zhong, Y. Fan, A novel cu-based covalent organic framework with cu–N_2O_2 single sites for efficient CO_2 electroreduction to methane, Appl. Catal. Environ. 354 (2024) 124145, https://doi.org/10.1016/j.apcatb.2024.124145.

[24] K. Boukheddaden, S. Miyashita, S. Triki, Spin transition materials: molecular and solid-state, J. Appl. Phys. 132 (2022) 220402, https://doi.org/10.1063/5.0135246.

[25] M.J. Al-Jeboori, A.H. Al-Dujaili, A.E. Al-Janabi, Coordination of carbonyl oxygen in the complexes of polymeric N-crotonyl-2-hydroxyphenylazomethine, Trans. Met. Chem. 34 (2009) 109–113. (b) M.J. Al-Jeboori, H.A. Hasan, W.A.J. Al-Sa'idy, Formation of polymeric chain assemblies of transition metal complexes with multidentate Schiff-base, Trans. Met. Chem. 34 (2009) 593–598.

[26] (a) A.T. Numan, M.J. Al-Jeboori, E.I. Abdulkarim, Synthesis and characterisation of novel ligand type N_2O_2 and its complexes with Cu, Co, Ni, Zn and Cd ions, J. Ibn Al-Haitham Pure Appl. Sci. 22 (2) (2009) 142–153. (b) M.J. Al-Jeboori, A.A. Ameer, N.A. Aboud, Novel pentadentate ligand of N_3S_2 donor atoms and its complexes with Ni^{2+}, Co^{2+}, Cu^{2+}, Fe^{2+}, Hg^{2+}, Ag^{+} and Re^{5+}, J. Ibn Al-Haitham Pure Appl. Sci. 17 (3) (2004) 80–97.

[27] A. Jana, B. Mohan, M. Choudhary, S. Dey, S. Kar, S.K. Das, Design, synthesis, and NLO properties of new Ni(II) and cu(II) complexes with extended Schiff base ligands: experimental and theoretical insights, J. Mol. Struct. 1328 (2024) 135312, https://doi.org/10.1016/j.molstruc.2024.135312.

[28] B. Mohan, A. Jana, N. Das, S. Bharti, M. Choudhary, S. Muhammad, S. Kumar, A. G. Al-Sehemi, H. Algarni, A dual approach to study the key features of nickel(II) and copper(II) coordination complexes: synthesis, crystal structure, optical and nonlinear properties, Inorg. Chim. Acta 484 (2019) 148–159, https://doi.org/10.1016/j.ica.2018.09.037.

[29] (a) N. Manurkar, M. Ilyas, F. Arshad, P. Patil, H. Shah, M.A. Khan, W. Hussain, H. Li, Exploring the first and second hyperpolarizabilities of l-glutamine-based Schiff base ligands and their cu(II) coordination complexes, New J. Chem. 49 (2025) 5200–5212, https://doi.org/10.1039/D5NJ00477B;
(b) K. Waszkowska, M. Busch, S. Slassi, A. Amine, A. El-Ghayoury, J. Strzelecki, A. Zawadzka, A.V. Kityk, P. Huber, B. Sahraoui, Transition-metal azo Schiff Base Complexes: nonlinear optics across solutions, thin films and nanocomposites, Adv. Opt. Mater. (2025), https://doi.org/10.1002/adom.202500975.

[30] L. von Wolf, E.G. Jäger, α-(Aminomethylen)-β-dicarbonylverbindungen als Komplexliganden. I. Kupfer- und Nickelchelate von Diaminderivaten, *Z. Anorg. Allg. Chem.* 346 (1966) 76–91. (b) E.F. Hasty, T.J. Colburn, D.N. Hendrickson, Copper(II) and vanadyl complexes of binucleating ligands. Magnetic exchange interactions propagated through an extensive organic system, *Inorg. Chem.* 12 (1973) 2414–2420.

[31] G.M. Sheldrick, *Acta Crystallogr.* C 75 (2019) 3–8.

[32] O.V. Dolomanov, L.J. Bourhis, R.J. Gildea, J.A.K. Howard, H. Puschmann, J. Appl. Cryst. 42 (2009) 339–341.

[33] Gaussian 16, Revision A.03, M.J. Frisch, G.W. Trucks, H.B. Schlegel, G.E. Scuseria, M.A. Robb, J.R. Cheeseman, G. Scalmani, V. Barone, G.A. Petersson, H. Nakatsuji, X. Li, M. Caricato, A.V. Marenich, J. Bloino, B.G. Janesko, R. Gomperts, B. Mennucci, H.P. Hratchian, J.V. Ortiz, A.F. Izmaylov, J.L. Sonnenberg, D. Williams-Young, F. Ding, F. Lipparini, F. Egidi, J. Goings, B. Peng, A. Petrone, T. Henderson, D. Ranasinghe, V.G. Zakrzewski, J. Gao, N. Rega, G. Zheng, W. Liang, M. Hada, M. Ehara, K. Toyota, R. Fukuda, J. Hasegawa, M. Ishida, T. Nakajima, Y. Honda, O. Kitao, H. Nakai, T. Vreven, K. Throssell, J.A. Montgomery Jr., J.E. Peralta, F. Ogliaro, M.J. Bearpark, J.J. Heyd, E.N. Brothers, K.N. Kudin, V.N. Staroverov, T.A. Keith, R. Kobayashi, J. Normand, K. Raghavachari, A.P. Rendell, J.C. Burant, S.S. Iyengar, J. Tomasi, M. Cossi, J.M. Millam, M. Klene, C. Adamo, R. Cammi, J.W. Ochterski, R.L. Martin, K. Morokuma, O. Farkas, J.B. Foresman, D.J. Fox, Gaussian 16, Revision A.03, Gaussian, Inc., Wallingford CT, 2016.

[34] L.H. Abdel-Rahman, M.T. Basha, B.S. Al-Farhan, et al., Synthesis, characterization, DFT studies of novel cu(II), Zn(II), VO(II), Cr(III), and La(III) chloro-substituted Schiff base complexes: aspects of its antimicrobial, antioxidant, anti-inflammatory, and photodegradation of methylene blue, Molecules 28 (2023) 4777, https://doi.org/10.3390/molecules28124777.

[35] (a) A.K. Singh, M.R. Patel, Conceptual DFT analysis of transition metal Schiff base complexes: insights into reactivity and stability, J. Mol. Struct. 1385 (2025) 131567;
(b) Y. Zhao, L. Wang, Frontier orbital and Fukui function analysis of VO(IV) and Cr(III) complexes with bioactive ligands, Inorg. Chim. Acta 558 (2025) 121234.

[36] M.J. Al-Jeboori, A.J. Abdul-Ghani, A.J. Al-Karawi, Synthesis and structural studies of new Mannich base ligands and their metal complexes, Trans. Met. Chem. 33 (2008) 925–930, https://doi.org/10.1007/s11243-008-9134-3.

[37] G. Ahumada, P. Hamon, T. Roisnel, V. Dorcet, M. Fuentealba, L.A. Hernández, D. Carrillo, J.-R. Hamon, C. Manzur, Spectroscopy, molecular structure, and electropolymerization of Ni(II) and cu(II) complexes containing a thiophene appending fluorinated Schiff base ligand, Dalton Trans. 52 (2023) 4224–4236, https://doi.org/10.1039/D3DT00224A.

[38] (a)R.M. Ahmed, E.I. Yousif, M.J. Al-Jeboori, Co(II) and cd(II) complexes derived from heterocyclic Schiff-bases: synthesis, structural characterisation, and biological activity, Sci. World J.: *Inorg. Chem.* (2013) (Article ID 754868 (6 pages).
(b) I.O. Issa, M.J. Al-Jeboori, J.S. Al-Dulaimi, Formation of binuclear metal complexes with multidentate Schiff-base oxime ligand: synthesis and spectral investigation, J. Ibn Al-Haitham Pure Appl. Sci. 24 (2) (2011) 142–153.

[39] (a)T.J. Al-Noor, M.J. Al-Jeboori, T. Mqeer, Synthesis and characterisation of the ligand (3,3′,4,4′-tetrakis(amido diacetyl monoxime) biphenyl) and its binuclear complexes with some metal ions, *Proc. 3rd Sci. Conf. Coll. Sci.*, Univ. Baghdad (2009) 1472–1481. (b) M.J. Al-Jeboori, A.A. Abdulrahman, S. Attia, Synthesis and characterization of novel ligand type N_2O_2 and its complexes with cu(II), co(II), Ni (II), Zn(II), and cd(II) ions, J. Ibn Al-Haitham Pure Appl. Sci. 18 (2) (2015) 51–67.

[40] (a) S.K. Gupta, G. Rajaraman, Magnetism in Ni(II) complexes: a combined experimental and theoretical perspective, Dalton Trans. 47 (2018) 5586–5601, https://doi.org/10.1039/C8DT00318A;
(b) M.A. Halcrow, Structure–magnetism relationships in molecular nickel(II) compounds, Coord. Chem. Rev. 253 (2009) 2493–2556, https://doi.org/10.1016/j.ccr.2009.01.014.

[41] (a) A. La Cour, M. Findeisen, R. Hazell, L. Hennig, C.E. Olsen, O. Simonsen, Nickel (II) N_2O_2 Schiff-base complexes incorporating pyrazole: syntheses, characterisation and acidity of the metal Centre towards co-ordinating solvents, J. Chem. Soc. Dalton Trans. (1996) 3437–3447, https://doi.org/10.1039/DT9960003437;
(b) R. Ahmad, M. Choudhary, Synthesis and design of manganese and nickel complexes with potential anticancer and antibacterial activities, and antiviral properties for therapeutic applications, New J. Chem. 49 (2025) 12401–12422, https://doi.org/10.1039/D5NJ00268K.

[42] (a) K. Wu, X. Huang, J. Yang, G. Zhang, J. Zhang, Y. Zhang, Y. Chen, J. Zhang, H. Wang, S. Zhang, J. Zhu, H. Chen, Q. Liu, Y. Lan, Z. Lei, Copper-catalyzed aerobic oxidative C-H/N–H coupling: From ketone and diamine to pyrazine, Sci. Adv. 1 (2015) e1500656, https://doi.org/10.1126/sciadv.1500656;
(b) B. Mitra, P. Ghosh, Copper catalysis for pyrazines and quinoxalines, in: P. Ghosh (Ed.), Copper in N-Heterocyclic Chemistry, Elsevier, 2021, pp. 221–248, https://doi.org/10.1016/B978-0-12-821263-9.00006-0;
(c) J. Li, Y. Yang, W. Hu, X. Xia, D. Wang, Catalytic synthesis of pyrazine and ketone derivatives by unsymmetrical triazolyl naphthyridinyl pyridine copper catalyst, Chin. J. Org. Chem. 42 (2022) 190–199, https://doi.org/10.6023/cjoc202107018.

[43] (a) L. Yang, D.R. Powell, R.P. Houser, Structural variation in copper(I) complexes with pyridylmethylamide ligands: structural analysis with a new four-coordinate geometry index, τ_4, Dalton Trans. (2007) 955–964, https://doi.org/10.1039/b617136b;
(b) A.W. Addison, T.N. Rao, J. Reedijk, J. van Rijn, G.C. Verschoor, Synthesis, structure, and spectroscopic properties of copper(II) compounds containing nitrogen–Sulphur donor ligands; the crystal and molecular structure of aqua[1,7-bis(N-methylbenzimidazol-2′-yl)-2,6-dithiaheptane]- copper(II) perchlorate, J. Chem. Soc. Dalton Trans. (1984) 1349–1356, https://doi.org/10.1039/DT9840001349;
(c) T. Guchhait, M. Giri, S.P. Mishra, Geometry indices for four- and five-coordinate metal complexes: a concise review, J. Coord. Chem. 77 (2024) 49–68.

[44] (a) F.H. Allen, O. Kennard, D.G. Watson, L. Brammer, A.G. Orpen, R. Taylor, Tables of bond lengths determined by X-ray and neutron diffraction. Part 1. Bond lengths in organic compounds, J. Chem. Soc. Perkin Trans. 2 (1987) S1–S19, https://doi.org/10.1039/P298700000S1;
(b) G. Udaya Kumar, K. Yadav, P. Mani, N. Sathishkumar, P. Suresh, Design, synthesis, X-ray, DFT, and molecular docking analysis of cu(II) complexes with N_2O_2 Schiff base ligands, Chem. Select. 6 (2021) 11504–11517, https://doi.org/10.1002/slct.202102822;
(c) P. Wang, L. Zhao, Synthesis and crystal structure of a supramolecular cu(II) complex based on N_2O_2 coordination sphere, Asian J. Chem. 27 (2015) 1424–1426.

[45] (a) J. Aihara, Reduced HOMO–LUMO gap as an index of kinetic stability for polycyclic aromatic hydrocarbons, *J. Phys. Chem.* A 103 (1999) 7487–7495, https://doi.org/10.1021/jp990092i;
(b) L.H. Madkour, S.K. Elroby, Inhibitive properties, thermodynamics, kinetics and quantum chemical calculations of polydentate Schiff base compounds as corrosion inhibitors for iron in acidic and alkaline media, Int. J. Ind. Chem. 6 (2015) 165–184, https://doi.org/10.1007/s40090-015-0039-7.

[46] (a) M. Alam, M.T.P. Beerepoot, K. Ruud, A generalised few-state model for the first hyperpolarizability, J. Chem. Phys. 152 (2020) 244106, https://doi.org/10.1063/5.0010231;
(b) M.U. Khan, M. Ibrahim, M. Khalid, A.A.C. Braga, S. Ahmed, A. Sultan, Prediction of second-order nonlinear optical properties of D–π–a compounds containing novel fluorene derivatives: a promising route to giant hyperpolarizabilities, J. Clust. Sci. 30 (2) (2019) 415–430, https://doi.org/10.1007/s10876-018-01489-1.

[47] Y. Takiguchi, Y. Onami, T. Haraguchi, T. Akitsu, Crystallographic and computational electron 9 of $d_{x^2-y^2}$ orbitals of azo-Schiff base metal complexes using conventional programs, Molecules 26 (2021) 551.

[48] (a) S.F. López, M.P. Meza, F.T. Hoyos, Study of the nonlinear optical properties of 4-nitroaniline type compounds by density functional theory calculations: towards new NLO materials, Comput. Theor. Chem. 1133 (2018) 25–32, https://doi.org/10.1016/j.comptc.2018.04.016;
(b) P. Selvaraj, K. Subramani, B. Srinivasan, C.-J. Hsu, C.-Y. Huang, Electro-optical effects of organic N-benzyl-2-methyl-4-nitroaniline dispersion in nematic liquid crystals, Sci. Rep. 10 (2020) 14273, https://doi.org/10.1038/s41598-020-71306-1.

[49] (a) F. Tessore, A.O. Biroli, G. Di Carlo, M. Pizzotti, Porphyrins for second-order nonlinear optics (NLO): an intriguing history, Inorganics 6 (2018) 81, https://doi.org/10.3390/inorganics6030081;
(b) T. Sutradhar, A. Misra, The role of π-linkers and electron acceptors in tuning the nonlinear optical properties of BODIPY-based zwitterionic molecules, RSC Adv. 10 (2020) 40300, https://doi.org/10.1039/d0ra02193h.
[50] M.G. Abd El-Nasser, T.I. Ismail, Synthesis, characterization, molecular docking studies, and theoretical calculations of novel Ni(II), Cu(II), and Zn(II) complexes based on benzothiazole derivative, BMC Chem. 19 (2025) 202, https://doi.org/10.1186/s13065-025-01576-1.
[51] (a) L. Rigamonti, A. Forni, E. Castiglioni, C. Baldoli, E. Licandro, S. Righetto, Chiral Schiff base metal complexes as second-order nonlinear optical chromophores: synthesis, characterization and DFT study, Materials 12 (2019) 1470, https://doi.org/10.3390/ma12091470;
(b) L. Rigamonti, A. Forni, E. Castiglioni, C. Baldoli, E. Licandro, S. Righetto, Unsymmetrically substituted Schiff base Ni(II) complexes: synthesis, structure and nonlinear optical properties, Dalton Trans. 48 (2019) 11905–11916, https://doi.org/10.1039/C9DT01958A.
[52] B. Rajasekhar, P.K. Muhammad Hijaz, T. Swu, Computational study on non-linear optical property of Wittig based Schiff-Base ligands (both Z E isomers) Copper(II) complex, J. Mol. Struct. 1168 (2018) 212–222, https://doi.org/10.1016/j.molstruc.2018.04.090.
[53] A. Karakaş, A. Elmali, Y. Elerman, Synthesis, crystal structure and nonlinear optical properties of a new cu(II) complex with a naphthyl Schiff base ligand, Spectrochim. Acta A Mol. Biomol. Spectrosc. 64 (2006) 1008–1013, https://doi.org/10.1016/j.saa.2005.08.020.
[54] S.R. Korupoju, K.H. Reddy, B.V. Reddy, Synthesis, characterization and nonlinear optical properties of a new triphenolic Schiff base and its cu(II) complex, Spectrochim. Acta A Mol. Biomol. Spectrosc. 152 (2016) 480–486, https://doi.org/10.1016/j.saa.2015.07.040.
[55] A. Trujillo, F. Justaud, L. Toupet, O. Cador, D. Carrillo, C. Manzur, J.-R. Hamon, New copper(II)-centered complexes with organometallic donor–acceptor substituted unsymmetrical Schiff base ligands, New J. Chem. 35 (2011) 2027–2036, https://doi.org/10.1039/c0nj01018a.
[56] S. Celedón, V. Dorcet, T. Roisnel, A. Singh, I. Ledoux-Rak, J.-R. Hamon, D. Carrillo, C. Manzur, Main-chain oligomers from Ni(II)- and cu(II)-centered unsymmetrical N_2O_2 Schiff-base complexes: synthesis and spectral, structural, and second-order nonlinear optical properties, Eur. J. Inorg. Chem. 2014 (2014) 4971–4981, https://doi.org/10.1002/ejic.201402469.

Prof. Dr. Mohamad J. Al-Jeboori is a Professor of Synthetic Inorganic Chemistry and Materials at the University of Baghdad, College of Education for Pure Science (Ibn Al-Haitham). He holds a Ph.D. in Synthetic Inorganic Chemistry for Radiopharmaceutical Applications and has over twenty-five years of experience in teaching and supervising postgraduate research in coordination chemistry, radiochemistry, and spectroscopy. His research focuses on ligand design, coordination complexes for biomedical and clean-energy applications, and CaO-based sorbents for CO_2 capture. Prof. Al-Jeboori is the author of more than 110 peer-reviewed publications and a co-inventor of a UK patent (GB 1114105.8) on calcium-looping CO_2 capture technology developed at Imperial College London.